

Cite this: *Chem. Sci.*, 2023, 14, 7665

All publication charges for this article have been paid for by the Royal Society of Chemistry

# Engineering ligand chemistry on Au<sub>25</sub> nanoclusters: from unique ligand addition to precisely controllable ligand exchange†

Jiangtao Zhao,<sup>a</sup> Abolfazl Ziarati,<sup>ID</sup> <sup>\*a</sup> Arnulf Rosspeintner,<sup>ID</sup> <sup>a</sup> Yanan Wang<sup>b</sup> and Thomas Bürgi<sup>ID</sup> <sup>\*a</sup>

Au<sub>25</sub> nanoclusters (NCs) protected by 18 thiol-ligands (Au<sub>25</sub>SR<sub>18</sub>, SR is a thiolate ligand) are the prototype of atomically precise thiolate-protected gold NCs. Studies concerning the alteration of the number of surface ligands for a given Au<sub>25</sub>SR<sub>18</sub> NC are scarce. Herein we report the conversion of hydrophobic Au<sub>25</sub>PET<sub>18</sub> (PET = 2-phenylethylthiolate) NCs to Au<sub>25</sub>SR<sub>19</sub> [Au<sub>25</sub>PET<sub>18</sub>(metal complex)<sub>1</sub>] induced by ligand exchange reactions (LERs) with thiolated terpyridine-metal complexes (metal complex, metal = Ru, Fe, Co, Ni) under mild conditions (room temperature and low amounts of incoming ligands). Interestingly, we found that the ligand addition reaction on Au<sub>25</sub>PET<sub>18</sub> NCs is metal dependent. Ru and Co complexes preferentially lead to the formation of Au<sub>25</sub>SR<sub>19</sub> whereas Fe and Ni complexes favor ligand exchange reactions. High-resolution electrospray ionization mass spectrometry (HRESI-MS) was used to determine the molecular formula of Au<sub>25</sub>SR<sub>19</sub> NCs. The photophysical properties of Au<sub>25</sub>PET<sub>18</sub>(Ru complex)<sub>1</sub> are distinctly different from Au<sub>25</sub>PET<sub>18</sub>. The absorption spectrum is drastically changed upon addition of the extra ligand and the photoluminescence quantum yield of Au<sub>25</sub>PET<sub>18</sub>(Ru complex)<sub>1</sub> is 14 times and 3 times higher than that of pristine Au<sub>25</sub>PET<sub>18</sub> and Au<sub>25</sub>PET<sub>17</sub>(Ru complex)<sub>1</sub>, respectively. Interestingly, only one surface ligand (PET) could be substituted by the metal complex when neutral Au<sub>25</sub>PET<sub>18</sub> was used for ligand exchange whereas two ligands could be exchanged when starting with negatively charged Au<sub>25</sub>PET<sub>18</sub>. This charge dependence provides a strategy to precisely control the number of exchanged ligands at the surface of NCs.

Received 3rd March 2023

Accepted 14th June 2023

DOI: 10.1039/d3sc01177a

rsc.li/chemical-science

## Introduction

Thiolate-protected metal nanoclusters (NCs) have attracted tremendous attention in the past few decades,<sup>1–4</sup> and triggered extensive research interests in many emerging fields, such as biological applications,<sup>5,6</sup> electro(photo)catalysis for energy conversion<sup>7,8</sup> and sensing,<sup>9,10</sup> owing to well-defined structures, unique optical and molecular-like properties.<sup>11</sup> To date, dozens of different thiolate-protected gold NCs are known (denoted as Au<sub>m</sub>SR<sub>n</sub>, *m* and *n* indicate the number of gold atoms and thiolate ligands, respectively), such as Au<sub>25</sub>SR<sub>18</sub>, Au<sub>38</sub>SR<sub>24</sub>, Au<sub>102</sub>SR<sub>44</sub>, Au<sub>144</sub>SR<sub>60</sub>, *etc.*<sup>12</sup> However, to further extend the range of possible applications of NCs, the research on diversification of Au NC species with modified morphologies and properties remains important.

Thiolate-ligands on the surface of the Au NCs play an important role during the synthesis of NCs,<sup>13</sup> and influence the physicochemical properties of NCs, boost their functionalities and affect the NC size.<sup>14–16</sup> The number of surface ligands for a given Au nuclearity is typically well-defined. For example, Au<sub>25</sub>SR<sub>18</sub>, the prototypical thiolate-protected gold NC contains exactly 18 ligands (the Au<sub>13</sub> core is surrounded by 6 Au<sub>2</sub>SR<sub>3</sub> staples). This NC seems the ideal candidate to study the derivatization chemistry of Au NCs. Nowadays, Au NCs are usually fabricated by a well-recognized synthetic method using neutral or anionic thiolate ligands, such as 2-phenylethanethiol (PET), glutathione, mercaptocarboxylic acids and so on.<sup>17–19</sup> The direct synthesis of cationic-ligand-protected Au NCs is limited because of coulombic attractions between the anionic Au ion (AuCl<sub>4</sub><sup>−</sup>) and the cationic thiol and coulombic repulsions caused by abundant cationic ligands at the surface of Au NCs.<sup>20,21</sup> Ligand exchange reactions (LERs), in which surface ligands on Au NCs are substituted with new thiolate ligands, thus functionalizing the NCs, provide a crucial post-synthesis methodology for surface chemical modification of Au NCs.<sup>22,23</sup> Particularly, chromophore-functionalized Au NCs were prepared and their photophysical properties studied.<sup>24–27</sup> For instance, the optical behavior was investigated in porphyrin functionalized chiral

<sup>a</sup>Department of Physical Chemistry, University of Geneva, 30 Quai Ernest-Ansermet, 1211, Geneva 4, Switzerland. E-mail: abolfazl.ziarati@unige.ch; thomas.buergi@unige.ch

<sup>b</sup>Department of Chemical Engineering, University of Michigan, Ann Arbor, 2800, MI, USA

† Electronic supplementary information (ESI) available. See DOI: <https://doi.org/10.1039/d3sc01177a>

$\text{Au}_{38}\text{SR}_{24}$  NC,<sup>28</sup> and a directional electron transfer from the  $\text{Au}_{25}$  NC to the pyrene was studied in pyrene-coupled  $\text{Au}_{25}$  NCs.<sup>29</sup> In addition, the ligand-exchange position controlled by steric hindrance of incoming ligands was revealed in porphyrin-thiol-substituted  $\text{Au}_{25}$  NCs system.<sup>30</sup> Ligand exchange with free ligand can be divided into two categories: (i) part or all surface ligands are replaced by the new ligands without changing the size and structure of the original Au NCs;<sup>31</sup> (ii) ligand exchange induces a size/structure transformation, which was reported by Jin and co-workers.<sup>32</sup> It provided an easy way to explore the diversity of NCs and generate new NCs with different composition and properties and to study the transformation mechanisms,<sup>33</sup> for example, from  $\text{Au}_{25}\text{SR}_{18}$  to  $\text{Au}_{28}\text{SR}'_{20}$ ,<sup>34</sup> from  $\text{Au}_{144}\text{SR}_{60}$  to  $\text{Au}_{133}\text{SR}'_{52}$ , and so on.<sup>35</sup> Some of us previously reported the transformation from  $\text{Au}_{25}\text{SR}_{18}$  to  $\text{Au}_{28}\text{SR}_{21}$  induced by LER with a chiral ligand under mild conditions in organic phase.<sup>36</sup> Xie and co-workers recently discovered a new hydrophilic  $\text{Au}_{25}\text{SR}_{19}$  NC by adding excess thiolate ligands (MHA = 6-mercaptophexanoic acid) to  $\text{Au}_{25}\text{MHA}_{18}$  NCs,<sup>37</sup> and the transformation mechanism was studied and proposed to occur through an oxidative etching process. In that work, the additional ligand was identical to the one protecting the original NC and the ligand addition process involving different ligands was not investigated.

In this work, we successfully obtained hydrophobic  $\text{Au}_{25}\text{SR}_{19}$  by precisely adding one metal complex as ligand on the  $\text{Au}_{25}\text{PET}_{18}$  surface. We demonstrated that the single ligand addition on  $\text{Au}_{25}\text{PET}_{18}$  is metal dependent (metal = Ru, Fe, Co, Ni), so that the ligand addition reaction can be precisely controlled. Time-resolved high resolution ESI and UV-vis spectra were recorded to monitor the transformation process of  $\text{Au}_{25}\text{SR}_{19}$ , and a structure of the  $\text{Au}_{25}\text{SR}_{19}$  NC is also proposed. Furthermore, it is worth to mention that neither excess thiolate ligand nor high temperature was needed to trigger this transformation. More interestingly, the number of surface ligands that can be replaced by metal complexes during LER depended on the charge of parent Au NCs.

## Results and discussions

Neutral  $\text{Au}_{25}\text{PET}_{18}$  (PET = 2-phenylethanethiol) was fabricated and purified according to previous reports and used as model NC in the following experiments.<sup>38</sup> UV-vis absorption spectra (ESI, Fig. S1a†) and high-resolution electrospray ionization mass spectra (HRESI-MS) (ESI, Fig. S1b†) of as-prepared neutral  $\text{Au}_{25}\text{PET}_{18}$  NC indicates successful synthesis and high purity.<sup>38,39</sup> ESI, Fig. S2† shows  $^1\text{H-NMR}$  spectra of the Ru complex. Characteristic absorption spectra and ESI-MS of different metal complexes are displayed in ESI, Fig. S3 and Table. S1,† respectively. LER was performed by mixing  $\text{Au}_{25}\text{PET}_{18}$  in dichloromethane and metal complex in acetonitrile (Fig. 1) in a glovebox at room temperature at NC/complex ratios of 1 : 2 and 1 : 4, respectively. The progress of the reaction was monitored by HRESI-MS (Fig. 2) at NC/complex ratio 1 : 2. Peak 5 at  $m/z = 7394.2$  and peak 4 located at  $m/z = 6058$  are assigned to the unreacted  $\text{Au}_{25}\text{PET}_{18}$  and its prominent fragment.

Fig. 2a shows the time-dependent ESI-MS during LER with the Ru complex at a ratio of 1 : 2, both experimental and simulated spectra of the emerging products are shown in Fig. 2b. As demonstrated in Fig. 2a and b, peak 2 and peak 3 are associated with doubly charged species because the interval between isotopic peaks is 0.5  $m/z$ . Peak 2 at  $m/z = 3965.9$  indicates that one PET ligand was substituted by the Ru complex,  $[\text{Au}_{25}\text{PET}_{17}(\text{Ru complex})_1]^{2+}$ . The isotopic pattern of peak 3 from  $m/z = 4030$  to  $m/z = 4044$  demonstrates that two species overlapped in this region, the right part at  $m/z = 4038.3$  is also consistent with one ligand exchange species, but containing one counterion  $\text{PF}_6^-$ . The left part located at  $m/z = 4034.5$  is assigned to a species containing one incoming ligand (Ru complex) added to  $\text{Au}_{25}\text{PET}_{18}$ ,  $[\text{Au}_{25}\text{PET}_{18}(\text{Ru complex})_1]^{2+}$ , a species with the same nuclearity but different ligand number. Noteworthy, peak 1 at  $m/z = 3366.1$  represents the fragment from  $\text{Au}_{25}\text{PET}_{18}(\text{Ru complex})_1$ , after losing  $\text{Au}_4\text{PET}_4$ . Such fragmentation is a common phenomenon for Au NCs during MS analysis.<sup>36</sup>

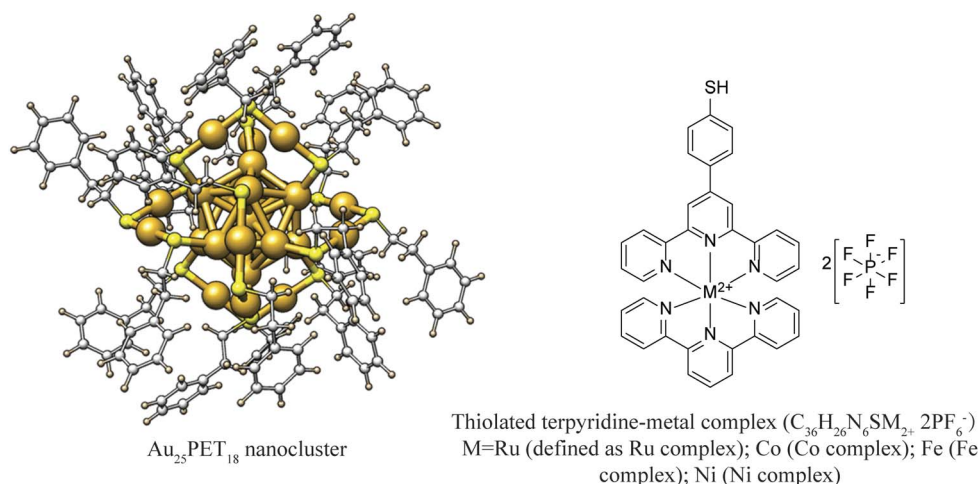


Fig. 1 Schematic diagram of  $\text{Au}_{25}\text{PET}_{18}$  NC and thiolated terpyridine-metal complex (counter ions:  $2\text{PF}_6^-$ ).

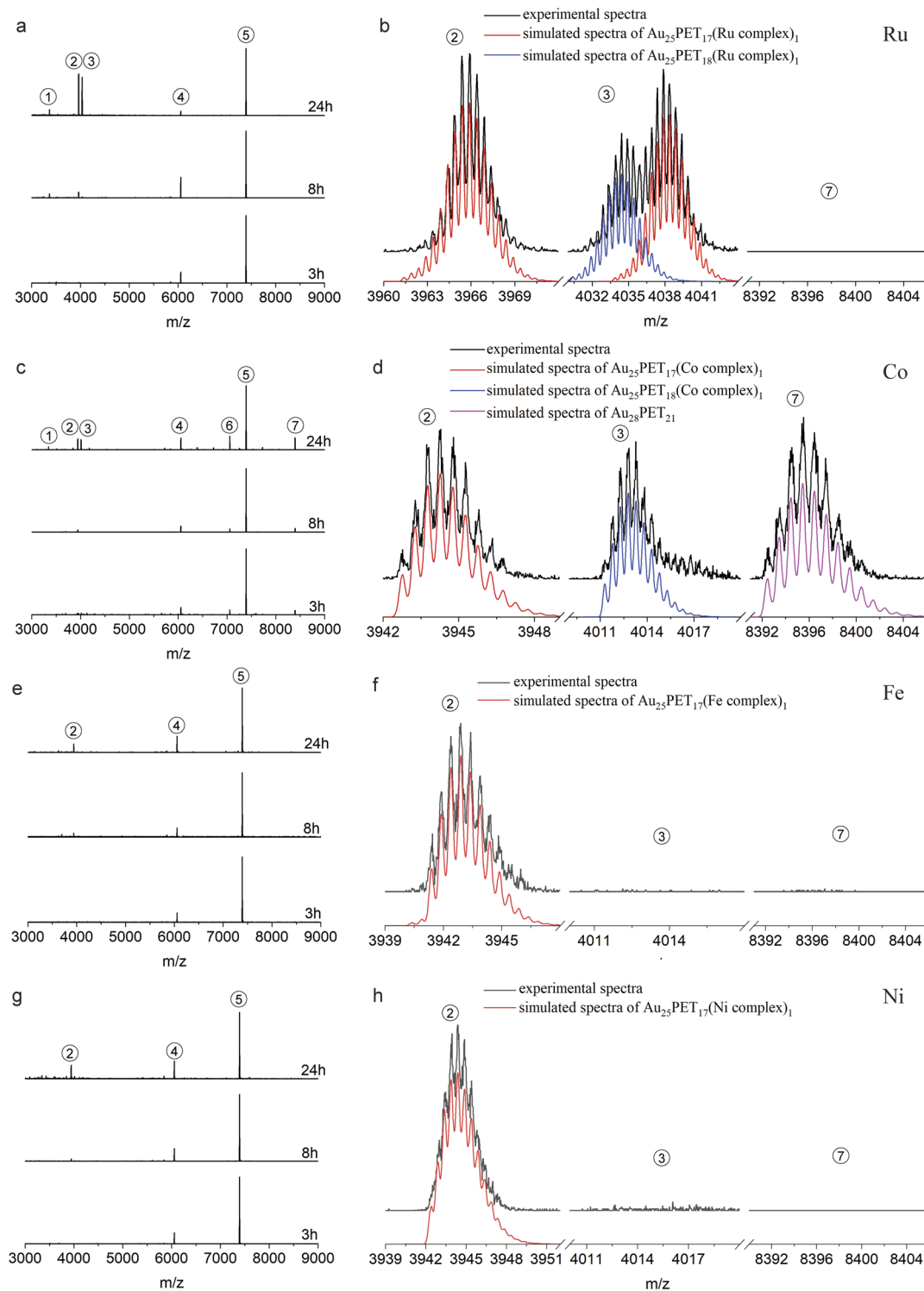


Fig. 2 Time-dependent ESI-MS during LER with Ru complex (a and b), Co complex (c and d), Fe complex (e and f) and Ni complex (g and h) at NCs/complex ratio 1 : 2. (b, d, f and h) Show the comparison of experimental and simulated isotopic patterns of different species after reaction for 24 h (enlarged from a, c, e and g, respectively). (Isotopic patterns distance = 0.5 in peak 1–3 indicated the charge  $z = 2+$ , distance = 1 in peak 4–7 showed the charge  $z = 1+$ ; the spectra are normalized with respect to peak 5).

Fig. 2c and d show the time-dependent HRESI-MS for the reaction with Co complex including detail views of some selected peaks. Peak 2 at  $m/z = 3944.8$  in Fig. 2c and its isotopic pattern in Fig. 2d indicates a NC where one surface ligand was

replaced by a Co complex,  $[\text{Au}_{25}\text{PET}_{17}(\text{Co complex})_1]^{2+}$ . In addition, comparison of the experimental isotope pattern of peak 3 at  $m/z = 4013.4$  and the simulated curve of  $\text{Au}_{25}\text{PET}_{18}(\text{Co complex})_1$  in Fig. 2d, also confirmed ligand addition. Peak 1 at



**Table 1** Summary of metal-dependent products after LER for 24 h at NC/complex ratio 1 : 2. (✓ means the reaction can take place, ✗ indicates that the reaction was not observed)

	Ru	Co	Fe	Ni
Ligand exchange reaction	✓	✓	✓	✓
Ligand addition reaction	✓	✓	✗	✗
Au <sub>28</sub> PET <sub>21</sub>	✗	✓	✗	✗

$m/z = 3344.8$  is a fragment from the Au<sub>25</sub>PET<sub>18</sub> (Co complex)<sub>1</sub> NC after loss of Au<sub>4</sub>PET<sub>4</sub>. More interestingly, the perfect matching of simulated isotope pattern and the experimental curve for the species at  $m/z = 8396.8$  indicates the formation of Au<sub>28</sub>PET<sub>21</sub> (peak 7 in Fig. 2c and d). Peak 6 at  $m/z = 7059.4$  could be due to the fragment from unreacted Au<sub>25</sub>PET<sub>18</sub> after loss of Au<sub>1</sub>PET<sub>1</sub> and Au<sub>28</sub>PET<sub>21</sub> after loss of Au<sub>4</sub>PET<sub>4</sub>. ESI-MS results after reaction for 3 h, 8 h and 24 h with Fe complex and Ni complex are shown in Fig. 2e, f, g and h, respectively. Both peak 2 in Fig. 2e and f at  $m/z = 3943.2$  and peak 2 in Fig. 2g and h at  $m/z = 3944.7$  correspond to ligand substitution with Fe complex and Ni complex, [Au<sub>25</sub>PET<sub>17</sub>(Fe complex)<sub>1</sub>] and Au<sub>25</sub>PET<sub>17</sub>(Ni

complex)<sub>1</sub>], respectively. Thus, the ligand-exchange species is the dominant product when reacting Au<sub>25</sub>PET<sub>18</sub> with Fe and Ni complex at a ratio of 1 : 2. Neither ligand addition nor size transformation was observed.

Table 1 summarizes the metal-dependent products after LER for 24 h at a NC/complex ratio of 1 : 2. It clearly shows that Ru and Co complexes can induce both ligand exchange and ligand addition on Au<sub>25</sub>PET<sub>18</sub>, and the transformation from Au<sub>25</sub> to Au<sub>28</sub> also appeared in the case of the Co complex. Nevertheless, only ligand-exchange products were observed when reacting with Fe and Ni complexes.

The reactions were also studied at a 1 : 4 NC: complex ratio (Fig. 3). Compared with the reactions at 1 : 2 ratio, Fig. 3a (reaction with Ru complex) and Fig. 3b (reaction with Co complex) show that a higher amount of metal complex is more favorable to induce the ligand addition on Au<sub>25</sub>PET<sub>18</sub>, forming Au<sub>25</sub>SR<sub>19</sub>. Noticeably, peak 3 in Fig. 3a and b after 24 h reaction, located at  $m/z = 4034.5$  and  $m/z = 4013.4$ , are still assigned to Au<sub>25</sub>SR<sub>19</sub>, [Au<sub>25</sub>PET<sub>18</sub>(Ru complex)<sub>1</sub>]<sup>2+</sup> and [Au<sub>25</sub>PET<sub>18</sub>(Co complex)<sub>1</sub>]<sup>2+</sup>, respectively. Moreover, peak 8 in Fig. 3b appearing at  $m/z = 4014.6$  ( $z = 2+$ ) indicates a new NC species corresponding to the addition of one Co complex to Au<sub>28</sub>PET<sub>21</sub>,

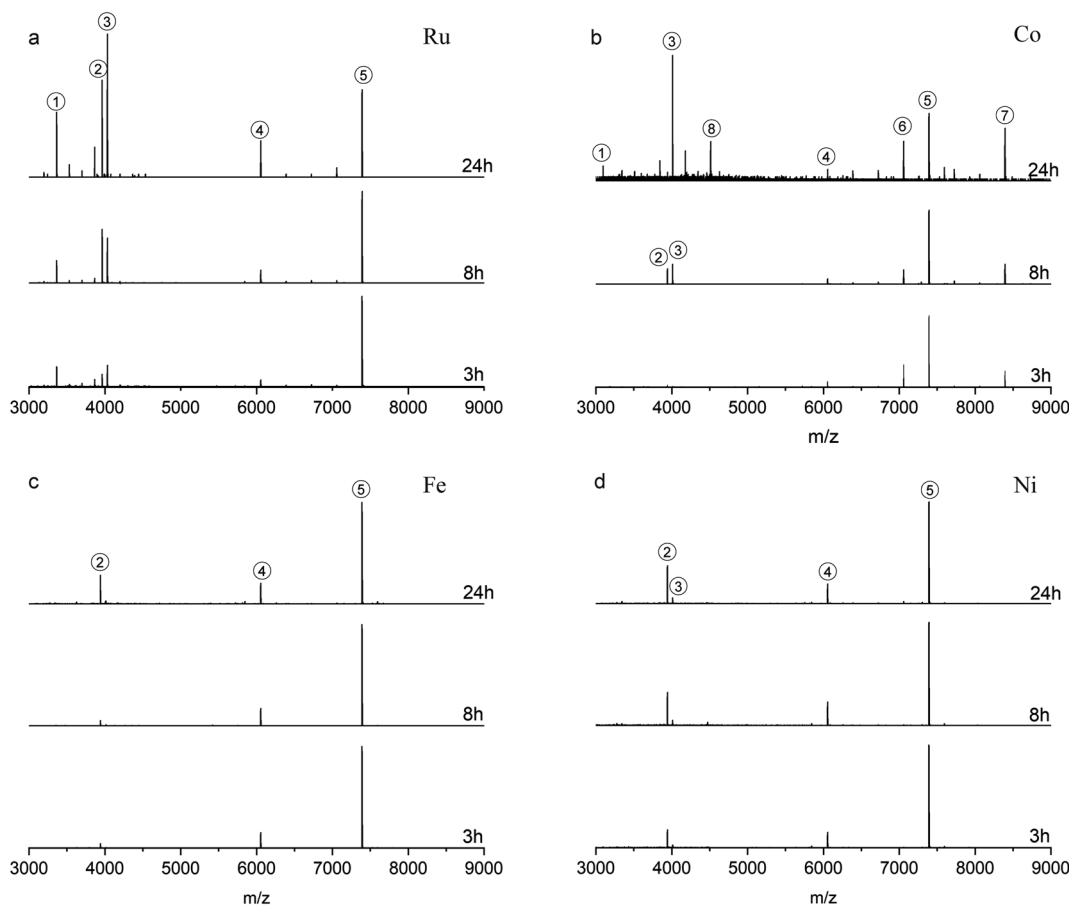


**Fig. 3** ESI-MS after reaction with Ru complex (a), Co complex (b), Fe complex (c), Ni complex (d) at NCs/complex ratio 1 : 4 (the spectra are normalized with respect to peak 5).



$[\text{Au}_{28}\text{PET}_{21}(\text{Co complex})_1]^{2+}$ , also demonstrating the ligand addition reaction for another NC. Concerning LER with Fe and Ni complex at 1 : 4 ratio, ligand-exchange species  $\text{Au}_{25}\text{PET}_{17}(\text{Metal complex})_1$  is still the main product (shown in Fig. 3c and d). Peak 3 in Fig. 3d at  $m/z = 4013.3$  confirmed that a small amount of  $\text{Au}_{25}\text{SR}_{19}$ ,  $[\text{Au}_{25}\text{PET}_{18}(\text{Ni complex})_1]^{2+}$ , formed during the reaction with Ni complex at high ratio.

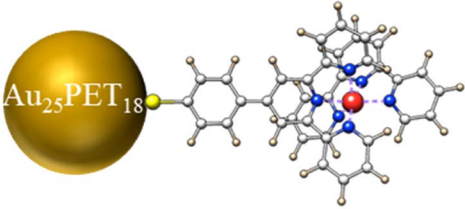
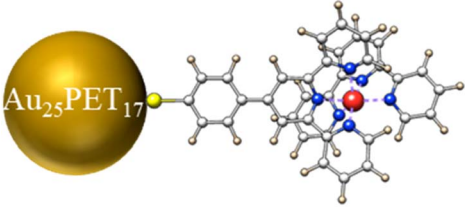

Since the Ru complex can induce both ligand exchange and ligand addition reactions, it was selected to further investigate the ligand addition process during LER at a 1 : 10 NC : complex ratio. HRESI-MS (ESI, Fig. S4†) indicates that most of the initial  $\text{Au}_{25}\text{PET}_{18}$  was converted to  $\text{Au}_{25}\text{SR}_{19}$  (peak 1 at 3366.1 and peak 3 at 4034.5) after 24 h, demonstrating that excess ligand is beneficial for the formation of  $\text{Au}_{25}\text{SR}_{19}$ , and the addition of a second complex was not observed.

In order to make sure that the ESI-MS signal of  $\text{Au}_{25}\text{SR}_{19}$  is not due to non-covalent interaction ( $\pi$ - $\pi$  stacking) between the surface ligand of  $\text{Au}_{25}\text{PET}_{18}$  and was prepared and mixed with  $\text{Au}_{25}\text{PET}_{18}$ . After reaction for 24 h, the sample was analyzed by HRESI-MS (ESI, Fig. S5†). The ESI mass spectra do not show the peak at  $m/z = 3959.8$  which is assigned to the ligand addition. This indicates that the ligand is added through covalent bonding and not through  $\pi$ - $\pi$  interaction.

Table 2 summarizes the proposed species and their corresponding  $m/z$  peaks based on the results in Fig. 2 and 3. Ru and Co complexes favor ligand addition (peak 3) reaction. The Co complex can also induce the transformation from  $\text{Au}_{25}$  to  $\text{Au}_{28}$  (peak 7) during LER. Nevertheless, with Fe and Ni complexes, ligand exchange (peak 2) is the preferred reaction.

A change of the ligand number while keeping the number of gold atoms constant will unavoidably affect the structure of the ligand shell and thus the properties of the whole NC. To study the photophysical properties,  $\text{Au}_{25}\text{SR}_{19}$  [ $\text{SR}_{19} = \text{PET}_{18}(\text{Ru complex})_1$ ] was prepared at a NC/Ru complex ratio of 1 : 10 and purified by silica column chromatography with eluents dichloromethane and acetonitrile (3 : 1). HRESI-MS indicated good purity (Fig. 4a). The isotope patterns located at  $m/z = 4034.5$  and  $m/z = 3366.1$  (Fig. 4b) match perfectly with simulated spectra of  $\text{Au}_{25}\text{SR}_{19}$  and its fragment after losing  $\text{Au}_4\text{PET}_4$ , which confirmed the molecular formula of  $\text{Au}_{25}\text{PET}_{18}(\text{Ru complex})_1$ . Fig. 4c shows some fragment peaks from  $\text{Au}_{25}\text{SR}_{19}$  and the isotope patterns. The peak at  $m/z = 406.0$  originates from the fragment  $\text{PET} + \text{Ru complex}$  [ $[\text{C}_8\text{H}_9\text{S}-\text{SC}_{36}\text{H}_{25}\text{N}_6\text{Ru}]^{2+}$ ]. In addition, the peak located at  $m/z = 937.1$  is assigned to  $[\text{Au}_4\text{PET}_3(\text{Ru complex})_1]^{2+}$ . Comparing the simulated isotopic patterns of  $\text{Au}_{25}\text{SR}_{19}$  for covalent and noncovalent attachment of the metal complex with the experimental mass spectra (ESI, Fig. S10†) shows that the simulated isotopic patterns for the covalent attachment matches well the experiment, thus indicating a covalent binding of the metal complex to the cluster. The observed  $\text{Au}_4\text{SR}_4$  fragment in ESI-MS may originate from staples ( $\text{SR}-\text{Au}-\text{SR}-\text{Au}-\text{SR}$ ) of the NC *e.g.* from multistep rearrangement of two or more staples on the surface of the NC prior to fragmentation.<sup>40,41</sup> A possible structure of  $\text{Au}_{25}\text{SR}_{19}$  was already proposed by Xie *et al.*, which is characterized by the removal of one Au atom from the  $\text{Au}_{13}$  core and the formation of a  $\text{Au}_3\text{SR}_4$  staple.<sup>37</sup>

Table 2 Proposed species and its corresponding ESI-MS peaks. S atoms are presented in yellow, z means charge

Species	$m/z$
Ligand addition	
	( $z = 2+$ ), $M = \text{Ru}$ : 4034.5, $M = \text{Co}$ : 4013.4, peak 3
Ligand exchange	
	( $z = 2+$ ), $M = \text{Ru}$ : 3965.9, $M = \text{Co}$ : 3944.8, $M = \text{Fe}$ : 3943.2, $M = \text{Ni}$ : 3944.7, peak 2
	( $z = 2+$ ), 8396.8, peak 7
Ligand addition- $\text{Au}_4\text{PET}_4$	( $z = 2+$ ), $M = \text{Ru}$ : 3366.1, $M = \text{Co}$ : 3344.8, peak 1





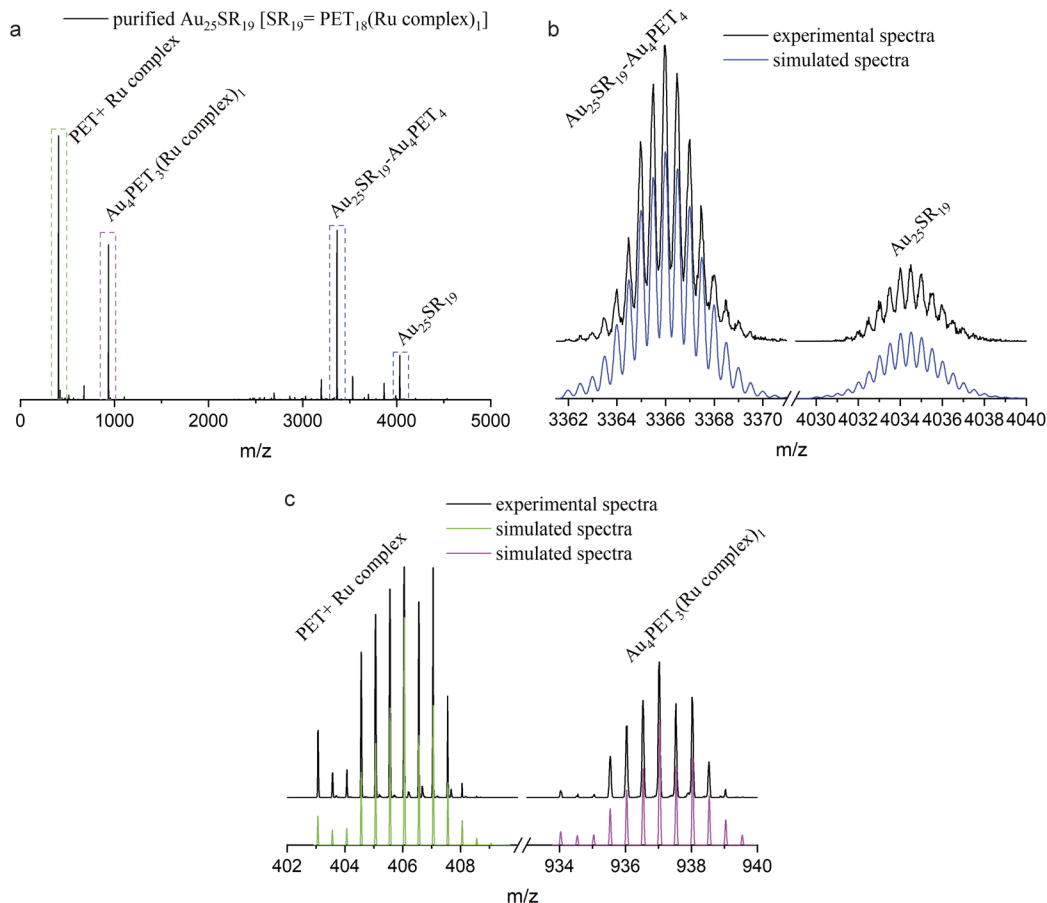


Fig. 4 (a) ESI-MS of  $\text{Au}_{25}\text{SR}_{19}$  [ $\text{SR}_{19} = \text{PET}_{18}(\text{Ru complex})_1$ ] after purification; (b) and (c): detailed isotopic peaks (in the square in a) and simulated isotopic patterns of labeled species, peak distance = 0.5.

The molar decadic extinction coefficient and differential luminescence quantum yield for  $\text{Au}_{25}\text{PET}_{18}$ ,  $\text{Au}_{25}\text{PET}_{17}(\text{Ru complex})_1$ , and  $\text{Au}_{25}\text{SR}_{19}$  [ $\text{SR}_{19} = \text{PET}_{18}(\text{Ru complex})_1$ ] are studied in Fig. 5a and b, respectively. As shown in Fig. 5a, the characteristic peaks from  $\text{Au}_{25}\text{SR}_{18}$  still remained in the ligand-exchange product [ $\text{Au}_{25}\text{PET}_{17}(\text{Ru complex})_1$ ], but disappeared

after ligand addition [ $\text{Au}_{25}\text{PET}_{18}(\text{Ru complex})_1$ ]. The intense peak at around 484.5 nm (2.56 eV) due to the Ru complex appeared in both  $\text{Au}_{25}\text{PET}_{17}(\text{Ru complex})_1$  and  $\text{Au}_{25}\text{PET}_{18}(\text{Ru complex})_1$ , confirming that the Ru complex was associated with the NC.

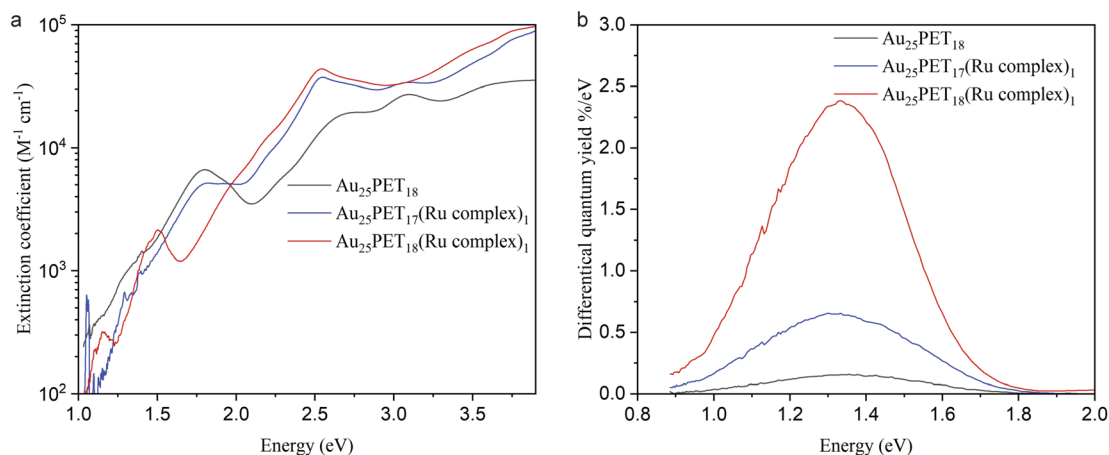


Fig. 5 (a) The extinction coefficient for  $\text{Au}_{25}\text{PET}_{18}$ ,  $\text{Au}_{25}\text{PET}_{17}(\text{Ru complex})_1$ , and  $\text{Au}_{25}\text{SR}_{19}$  [ $\text{SR}_{19} = \text{PET}_{18}(\text{Ru complex})_1$ ]; (b) spectra of the differential luminescence quantum yield for  $\text{Au}_{25}\text{PET}_{18}$ ,  $\text{Au}_{25}\text{PET}_{17}(\text{Ru complex})_1$  and  $\text{Au}_{25}\text{PET}_{18}(\text{Ru complex})_1$ .



**Table 3** Luminescence quantum yield of Au<sub>25</sub>PET<sub>18</sub>, Au PET<sub>17</sub>(Ru complex)<sub>1</sub> and Au<sub>25</sub>PET<sub>18</sub>(Ru complex)<sub>1</sub>

	Quantum yield
Au <sub>25</sub> PET <sub>18</sub>	0.075%
Au PET <sub>17</sub> (Ru complex) <sub>1</sub>	0.32%
Au <sub>25</sub> PET <sub>18</sub> (Ru complex) <sub>1</sub>	1.05%

The extinction coefficient for Au<sub>25</sub>PET<sub>17</sub>(Ru complex)<sub>1</sub> and Au<sub>25</sub>PET<sub>18</sub>(Ru complex)<sub>1</sub> after subtraction of the contribution from the Ru complex are shown in ESI, Fig. S11.† Au<sub>25</sub>PET<sub>17</sub>(Ru complex)<sub>1</sub> exhibited very similar features compared with parent Au<sub>25</sub>PET<sub>18</sub>, while the spectrum of Au<sub>25</sub>PET<sub>18</sub>(Ru complex)<sub>1</sub> completely changed, indicating that the electronic structure of Au<sub>25</sub>PET<sub>18</sub>(Ru complex)<sub>1</sub> changed drastically compared to Au<sub>25</sub>PET<sub>18</sub>.

Interestingly, the luminescence spectra show very similar shape and peak position (Fig. 5b, ESI, Fig. S12† also shows emission spectra after normalization) for all three species Au<sub>25</sub>PET<sub>18</sub>, Au<sub>25</sub>PET<sub>17</sub>(Ru complex)<sub>1</sub> and Au<sub>25</sub>PET<sub>18</sub>(Ru complex)<sub>1</sub>. The emission peak for pure Ru complex appears at 670 nm (1.85 eV, ESI, Fig. S12†). However, after binding to Au<sub>25</sub> NCs, quenching of the chromophore fluorescence is observed, which can be due to energy transfer from the metal complex to the NC.<sup>28</sup> The luminescence peak at 1.33 eV for Au<sub>25</sub>PET<sub>18</sub>, Au<sub>25</sub>PET<sub>17</sub>(Ru complex)<sub>1</sub> and Au<sub>25</sub>PET<sub>18</sub>(Ru complex)<sub>1</sub> probably stems from the core of the Au NCs, indicating that the core is not changing after ligand addition. However, Au<sub>25</sub>PET<sub>18</sub>(Ru complex)<sub>1</sub> shows a drastic enhancement of quantum yield (Fig. 5b). Table 3 summarizes the luminescence quantum yields for these NCs. An increase of the luminescence quantum yield is observed for Au<sub>25</sub>PET<sub>18</sub>(Ru complex)<sub>1</sub> compared to the initial Au<sub>25</sub>PET<sub>18</sub>. All samples exhibit a violation of Kasha's rule, as the luminescence shows up at higher energy than the lowest energy absorption band.

To further investigate the mechanism for the ligand addition reaction, unreacted Au<sub>25</sub>PET<sub>18</sub> was separated from the reaction

mixture, as shown in Fig. 6a, and studied. Fig. 6b shows UV-vis spectra of the top and bottom parts of fraction 1. According to these spectra, the bottom part can be assigned to neutral Au<sub>25</sub>PET<sub>18</sub> (written as [Au<sub>25</sub>PET<sub>18</sub>]<sup>0</sup>), but in the UV-vis spectra of the top part, both peaks at around 400 nm and 700 nm were bleached, which indicates positively charged Au<sub>25</sub>PET<sub>18</sub> (written as [Au<sub>25</sub>PET<sub>18</sub>]<sup>+</sup>).<sup>42</sup> ESI-MS (Fig. 6c) was also applied to confirm the unreacted Au<sub>25</sub>PET<sub>18</sub> of fraction 1 (top part). Since neutral Au<sub>25</sub>PET<sub>18</sub> was used as the starting point for all ligand exchange reactions, however, both neutral and positively charged Au<sub>25</sub>PET<sub>18</sub> were observed after ligand addition, we propose that [Au<sub>25</sub>PET<sub>18</sub>]<sup>+</sup> should be the intermediate in the ligand addition reaction. Noteworthy, neutral Au<sub>25</sub>PET<sub>18</sub> cannot be oxidized to [Au<sub>25</sub>PET<sub>18</sub>]<sup>+</sup> on the silica column. Therefore, the transformation process from Au<sub>25</sub>SR<sub>18</sub> to Au<sub>25</sub>SR<sub>19</sub> is proposed as below: [Au<sub>25</sub>PET<sub>18</sub>]<sup>0</sup> is oxidized to [Au<sub>25</sub>PET<sub>18</sub>]<sup>+</sup>, then [Au<sub>25</sub>PET<sub>18</sub>]<sup>+</sup> NCs react with an external thiolate ligand to form a new isoelectric species, [Au<sub>25</sub>SR<sub>19</sub>]<sup>0</sup>, realizing the addition of one thiolate ligand to the original NC. The transformation mechanism is also consistent with the oxidation process proposed by Xie *et al.*<sup>37</sup> In our work, the ligand addition reaction is dependent on the metal cations in the complexes, which indicates that metals play an important role in the process of ligand addition. We hypothesize that Ru and Co complexes are able to oxidize neutral Au<sub>25</sub>PET<sub>18</sub> NCs to [Au<sub>25</sub>PET<sub>18</sub>]<sup>+</sup> (in contrast to Fe and Ni complexes), so that the ligand addition reaction can take place easily. Moreover, the reported reduction potentials for the addition of the first electron to [M(tpy)<sub>2</sub>]<sup>2+</sup> (M = Co, Ni, Fe, Ru; tpy = 2,2':6',2''-terpyridine)<sup>43,44</sup> indicate the following oxidant power of [M(tpy)<sub>2</sub>]<sup>2+</sup>: [Co(tpy)<sub>2</sub>]<sup>2+</sup> > [Ru(tpy)<sub>2</sub>]<sup>2+</sup> > [Fe(tpy)<sub>2</sub>]<sup>2+</sup> > [Ni(tpy)<sub>2</sub>]<sup>2+</sup>. This observation is also consistent with our hypothesis that Co and Ru complexes have stronger tendency to oxidize the NC.

Furthermore, we found that only one ligand at the surface could be replaced by metal complexes when neutral [Au<sub>25</sub>PET<sub>18</sub>]<sup>0</sup> was used for LERs. In order to shed light on this interesting phenomenon, we performed LER starting from negatively charged Au<sub>25</sub>PET<sub>18</sub> (written as [Au<sub>25</sub>PET<sub>18</sub>]<sup>−1</sup>) at a NC/

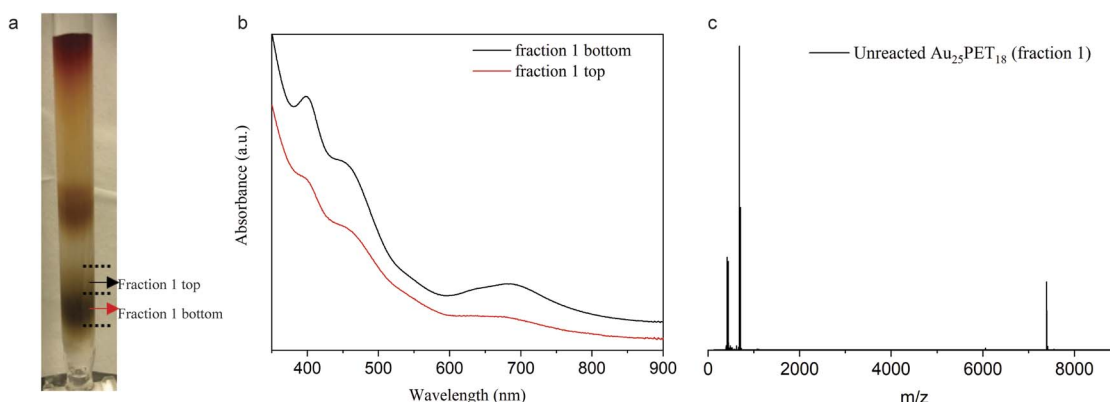


**Fig. 6** (a) Photograph of silica column after LER of Au<sub>25</sub>PET<sub>18</sub> with Ru complex for 24 h at NC/complex ratio 1 : 4, fraction 2 contains both ligand exchange and ligand addition products; (b) UV-vis spectra of fraction 1 (top part and bottom part, as indicated in a); (c) ESI-MS of fraction 1 top part.



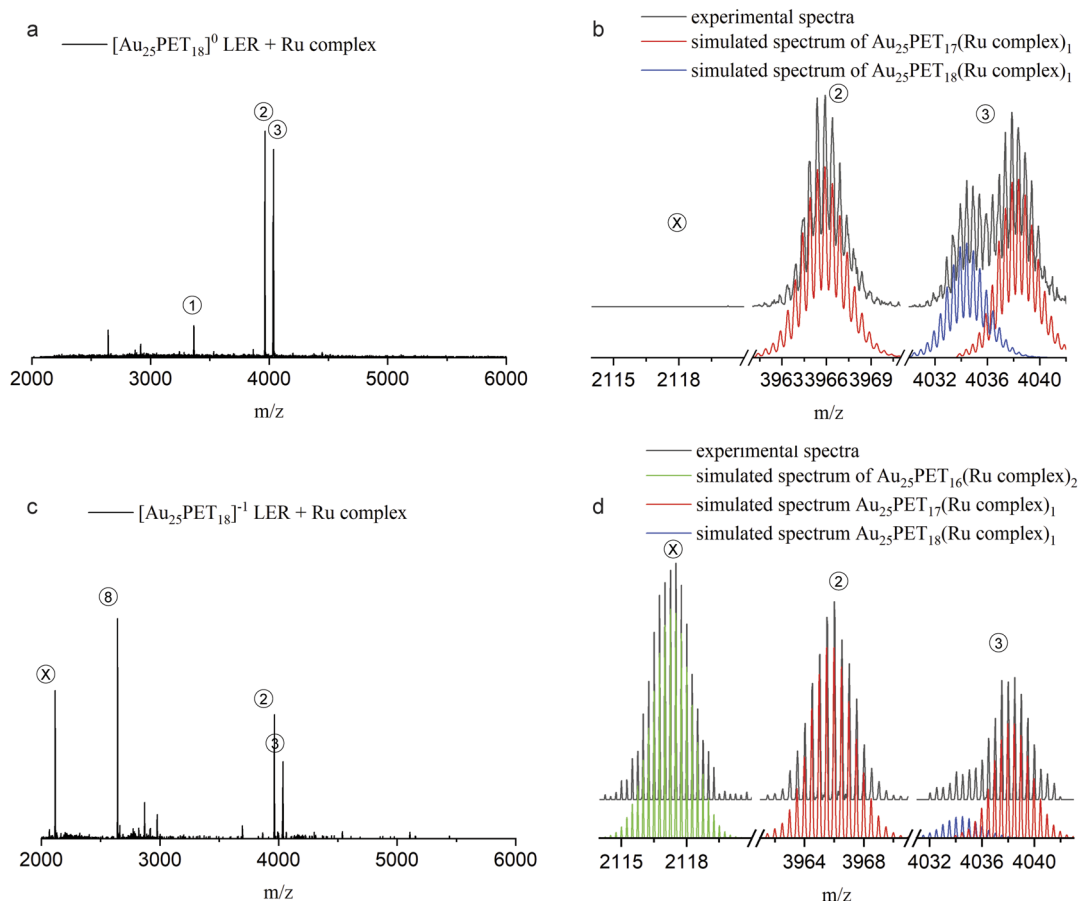


Fig. 7 ESI-MS after LER started from neutral Au<sub>25</sub>PET<sub>18</sub> (a and b) and negatively charged Au<sub>25</sub>PET<sub>18</sub> (c and d) with Ru complex at NC/complex ratio 1 : 2 for 24 h.

complex ratio of 1 : 2. Fig. 7 shows HRESI-MS and detailed isotopic patterns after mixing either [Au<sub>25</sub>PET<sub>18</sub>]<sup>0</sup> or [Au<sub>25</sub>PET<sub>18</sub>]<sup>-1</sup> with the Ru complex and reacting for 24 h. As shown in Fig. 7a and b, products related with one ligand exchange (peak 2 and right part of peak 3) and addition of only one ligand (left part of peak 3) were observed when LER started from [Au<sub>25</sub>PET<sub>18</sub>]<sup>0</sup>. Interestingly, when [Au<sub>25</sub>PET<sub>18</sub>]<sup>-1</sup> was used for LER with the Ru complex, the product of two ligand exchanges, Au<sub>25</sub>PET<sub>16</sub>(Ru complex)<sub>2</sub>, (peak X in Fig. 7c and d), was observed in addition to species resulting from one ligand exchange and ligand addition, respectively. The emerging peak X at *m/z* = 2117 (charge *z* = 4+) is assigned to [Au<sub>25</sub>PET<sub>16</sub>(Ru complex)<sub>2</sub>]<sup>4+</sup> (molecular formula: (Au<sub>25</sub>C<sub>200</sub>H<sub>194</sub>N<sub>12</sub>S<sub>18</sub>Ru<sub>2</sub>)<sup>4+</sup>). The measured and simulated isotope patterns shown in Fig. 7b match very well. Another prominent peak at *m/z* = 2643.9 matches a NC with one ligand exchanged but with *z* = 3+, [Au<sub>25</sub>PET<sub>17</sub>(Ru complex)<sub>1</sub>]<sup>3+</sup>. Based on these interesting results, we hypothesize that the number of the metal complexes that can be exchanged to the NCs is strongly related to the charge of parent NCs. The Au<sub>25</sub>SR<sub>18</sub> NC may be oxidized during LER with Ru complex, and easily accessible charge states for Au<sub>25</sub>SR<sub>18</sub> are -1, 0, +1. Therefore, only one ligand can be substituted by metal complex on initially neutral Au<sub>25</sub>PET<sub>18</sub>, but two on initially

negatively charged [Au<sub>25</sub>PET<sub>18</sub>]<sup>-</sup>. This could provide a promising method to precisely control the ligand-exchange number at the surface of NCs.

## Conclusions

In conclusion, Au<sub>25</sub>SR<sub>19</sub> was successfully obtained by precisely adding one thiolated terpyridine-metal complex to Au<sub>25</sub>PET<sub>18</sub> NCs during ligand exchange reaction at mild conditions. Moreover, we demonstrated that the reaction is metal dependent. Ru and Co complexes were favorable for ligand addition leading to Au<sub>25</sub>SR<sub>19</sub>, whereas Fe and Ni complexes promoted the exchange of one ligand. Also, NC/complex ratio and reaction time were studied, revealing that more metal complex and longer reaction time were advantageous for ligand addition on Au<sub>25</sub>. Therefore, the ligand addition process can be easily and precisely controlled. HRESI-MS also gave some hints concerning the structure of Au<sub>25</sub>SR<sub>19</sub>. The new NC showed different electronic structure and strongly enhanced luminescence compared with pristine Au<sub>25</sub>PET<sub>18</sub>. The manipulation of the number of ligands at a given Au NCs provides additional possibilities for the diversification of NCs and to change their physiochemical properties, thus boosting the application of Au





NCs. More interestingly, only one ligand can be replaced on neutral Au<sub>25</sub>PET<sub>18</sub> but two on negatively charged Au<sub>25</sub>PET<sub>18</sub> during LER with metal complexes, which provides us with a novel methodology to precisely control the ligand-exchange number at the surface of NCs.

Experimental section shown in ESI.†

## Data availability

The original data leading to this publication are available at <https://doi.org/10.5281/zenodo.8079142>.

## Author contributions

T. B. and A. Z. conceived the idea of the research. J. Z. performed all of the experiments, analysed data and wrote the manuscript with the help of Y. W., A. Z. and T. B. The photophysical experiment was conducted with the help of A. R. All authors contributed to editing the manuscript.

## Conflicts of interest

There are no conflicts to declare.

## Acknowledgements

T. B. acknowledges the generous support of the Swiss National Science Foundation (grant 200020\_192232) and the University of Geneva. The authors acknowledge the Mass Spectrometry core facility (MZ ChemBio). We thank Luis Llanes Montesino for help with the photoluminescence experiments. J. Z. would like to thank China Scholarship Council (CSC201807040048) for the financial supporting.

## Notes and references

- 1 R. Jin, C. Zeng, M. Zhou and Y. Chen, *Chem. Rev.*, 2016, **116**, 10346–10413.
- 2 A. W. Cook and T. W. Hayton, *Acc. Chem. Res.*, 2018, **51**, 2456–2464.
- 3 Q. Yao, X. Yuan, V. Fung, Y. Yu, D. T. Leong, D.-e. Jiang and J. Xie, *Nat. Commun.*, 2017, **8**, 927.
- 4 I. Chakraborty and T. Pradeep, *Chem. Rev.*, 2017, **117**, 8208–8271.
- 5 Y. Su, T. Xue, Y. Liu, J. Qi, R. Jin and Z. Lin, *Nano Res.*, 2019, **12**, 1251–1265.
- 6 J. Yang, Y. Peng, S. Li, J. Mu, Z. Huang, J. Ma, Z. Shi and Q. Jia, *Coord. Chem. Rev.*, 2022, **456**, 214391.
- 7 X. Cui, J. Wang, B. Liu, S. Ling, R. Long and Y. Xiong, *J. Am. Chem. Soc.*, 2018, **140**, 16514–16520.
- 8 S. Li, A. V. Nagarajan, D. R. Alfonso, M. Sun, D. R. Kauffman, G. Mpourmpakis and R. Jin, *Angew. Chem.*, 2021, **133**, 6421–6426.
- 9 L. Shang, J. Xu and G. U. Nienhaus, *Nano Today*, 2019, **28**, 100767.
- 10 J. Sun and Y. Jin, *J. Mater. Chem. C*, 2014, **2**, 8000–8011.
- 11 Y. Cao, T. Chen, Q. Yao and J. Xie, *Acc. Chem. Res.*, 2021, **54**, 4142–4153.
- 12 B. Kumar, T. Kawawaki, N. Shimizu, Y. Imai, D. Suzuki, S. Hossain, L. V. Nair and Y. Negishi, *Nanoscale*, 2020, **12**, 9969–9979.
- 13 Q. Yao, T. Chen, X. Yuan and J. Xie, *Acc. Chem. Res.*, 2018, **51**, 1338–1348.
- 14 Z. Gan, J. Chen, J. Wang, C. Wang, M.-B. Li, C. Yao, S. Zhuang, A. Xu, L. Li and Z. Wu, *Nat. Commun.*, 2017, **8**, 14739.
- 15 C. Zeng, Y. Chen, A. Das and R. Jin, *J. Phys. Chem. Lett.*, 2015, **6**, 2976–2986.
- 16 Y. Niihori, Y. Kikuchi, A. Kato, M. Matsuzaki and Y. Negishi, *ACS Nano*, 2015, **9**, 9347–9356.
- 17 H. Häkkinen, *Nat. Chem.*, 2012, **4**, 443–455.
- 18 X. Yuan, B. Zhang, Z. Luo, Q. Yao, D. T. Leong, N. Yan and J. Xie, *Angew. Chem.*, 2014, **126**, 4711–4715.
- 19 T. Bürgi, *Nanoscale*, 2015, **7**, 15553–15567.
- 20 Y. Ishida, K. Narita, T. Yonezawa and R. L. Whetten, *J. Phys. Chem. Lett.*, 2016, **7**, 3718–3722.
- 21 Z. Huang, Y. Ishida, K. Narita and T. Yonezawa, *J. Phys. Chem. C*, 2018, **122**, 18142–18150.
- 22 C. L. Heinecke, T. W. Ni, S. Malola, V. Mäkinen, O. A. Wong, H. Häkkinen and C. J. Ackerson, *J. Am. Chem. Soc.*, 2012, **134**, 13316–13322.
- 23 Y. Wang and T. Bürgi, *Nanoscale Adv.*, 2021, **3**, 2710–2727.
- 24 A. Dominguez-Castro, C. R. Lien-Medrano, K. Maghrebi, S. Messaoudi, T. Frauenheim and A. Fihey, *Nanoscale*, 2021, **13**, 6786–6797.
- 25 E. Hulkko, T. Lahtinen, V. Marjomaki, E. Pohjolainen, V. Saarnio, K. Sokolowska, A. Ajitha, M. Kuisma, L. Lehtovaara, G. Groenhof, H. Hakkinen and M. Pettersson, *Nanoscale Adv.*, 2021, **3**, 6649–6658.
- 26 K. Pyo, N. H. Ly, S. M. Han, M. B. Hatshan, A. Abuhagr, G. Wiederrecht, S. W. Joo, G. Ramakrishna and D. Lee, *J. Phys. Chem. Lett.*, 2018, **9**, 5303–5310.
- 27 R. K. Pandey, C. Chakraborty, U. Rana, S. Moriyama and M. Higuchi, *J. Mater. Chem. A*, 2016, **4**, 4398–4401.
- 28 B. Varnholt, R. Letrun, J. J. Bergkamp, Y. Fu, O. Yushchenko, S. Decurtins, E. Vauthey, S. X. Liu and T. Bürgi, *Phys. Chem. Chem. Phys.*, 2015, **17**, 14788–14795.
- 29 M. S. Devadas, K. Kwak, J.-W. Park, J.-H. Choi, C.-H. Jun, E. Sinn, G. Ramakrishna and D. Lee, *J. Phys. Chem. Lett.*, 2010, **1**, 1497–1503.
- 30 W. Suzuki, R. Takahata, Y. Chiga, S. Kikkawa, S. Yamazoe, Y. Mizuhata, N. Tokitoh and T. Teranishi, *J. Am. Chem. Soc.*, 2022, **144**, 12310–12320.
- 31 G. H. Woehrle, L. O. Brown and J. E. Hutchison, *J. Am. Chem. Soc.*, 2005, **127**, 2172–2183.
- 32 C. Zeng, C. Liu, Y. Pei and R. Jin, *ACS Nano*, 2013, **7**, 6138–6145.
- 33 M. P. Maman, A. S. Nair, H. Cheraparambil, B. Pathak and S. Mandal, *J. Phys. Chem. Lett.*, 2020, **11**, 1781–1788.
- 34 C. Zeng, T. Li, A. Das, N. L. Rosi and R. Jin, *J. Am. Chem. Soc.*, 2013, **135**, 10011–10013.
- 35 X. Kang and M. Zhu, *Chem. Mater.*, 2019, **31**, 9939–9969.



- 36 Y. Wang, B. Nieto-Ortega and T. Bürgi, *Chem. Commun.*, 2019, **55**, 14914–14917.
- 37 Y. Cao, V. Fung, Q. Yao, T. Chen, S. Zang, D.-e. Jiang and J. Xie, *Nat. Commun.*, 2020, **11**, 5498.
- 38 X. Kang, H. Chong and M. Zhu, *Nanoscale*, 2018, **10**, 10758–10834.
- 39 C. Comby-Zerbino, F. Bertorelle, P. Dugourd, R. Antoine and F. Chiot, *J. Phys. Chem. A*, 2020, **124**, 5840–5848.
- 40 R. Hamouda, F. Bertorelle, D. Rayane, R. Antoine, M. Broyer and P. Dugourd, *Int. J. Mass Spectrom.*, 2013, **335**, 1–6.
- 41 L. A. Angel, L. T. Majors, A. C. Dharmaratne and A. Dass, *ACS Nano*, 2010, **4**, 4691–4700.
- 42 D. R. Kauffman, D. Alfonso, C. Matranga, P. Ohodnicki, X. Deng, R. C. Siva, C. Zeng and R. Jin, *Chem. Sci.*, 2014, **5**, 3151–3157.
- 43 D. Ghosh, T. Kajiwar, S. Kitagawa and K. Tanaka, *Eur. J. Inorg. Chem.*, 2020, **2020**, 1814–1818.
- 44 N. Elgrishi, M. B. Chambers, V. Artero and M. Fontecave, *Phys. Chem. Chem. Phys.*, 2014, **16**, 13635–13644.

